Tuning Intercalation Sites in Nickel Hexacyanoferrate Using Lattice Nonstoichiometry

Xiaogang Hao† and Daniel T. Schwartz*,‡

Department of Chemical Engineering, Taiyuan University of Technology, 79 West Yinze Street, Taiyuan Shanxi 030024, People's Republic of China, and Electrochemical Materials and Interfaces Laboratory, Department of Chemical Engineering, Box 351750, University of Washington, Seattle, Washington 98195-1750

Received July 12, 2005. Revised Manuscript Received September 8, 2005

Reversible intercalation/deintercalation of K^+ in nickel hexacyanoferrate (NiHCF) thin films occurs in two energetically distinct, largely noninteracting, sites whose proportions are set by lattice nonstoichiometry. Principal component analysis (PCA) is used to correlate the stoichiometry of NiHCF, measured using energy-dispersive X-ray spectroscopy (EDS), with intercalation processes measured via cyclic voltammetry (CV). NiHCF voltammograms are well-known to exhibit two reversible peaks for K^+-containing electrolytes; each peak represents a different local cation intercalation/deintercalation environment. PCA of 59 different CV-EDS data sets shows (to first order) that the relative sizes of the two CV peaks are proportional to the lattice nonstoichiometry, but the peak locations (energies) are largely independent of stoichiometry. Intercalation sites in stoichiometric lattices are energetically favored compared to sites associated with defects ($\Delta G \approx -10$ kJ/mol K^+). The proportionality of CV peak sizes, and lack of peak shifting with lattice nonstoichiometry, indicates the different intercalation sites are largely noninteracting. Weak site−site interactions allow easy tuning of intercalation properties via lattice stoichiometry, though the best sensing or separation performance will likely be achieved in either defect-free lattices or highly nonstoichiometric lattices where, in each case, a single type of intercalation site is dominant. Processing conditions for creating a wide range of NiHCF lattice stoichiometries are presented.

Introduction

Nickel hexacyanoferrate (NiHCF), a nickel analogue of Prussian blue, can be formed as a thin film on conductive substrates via several synthesis routes.[1] Modulating the valence of the iron centers in thin films drives a reversible intercalation/deintercalation of charge-compensating alkali cations.[2] This trait has been exploited for sensors[3] and ion exchange.[4−6] Initially, thin films of NiHCF grown by anodic derivatization of nickel electrodes were thought to be structural analogues of "soluble" Prussian blue,[7−9] though a more complex view of the stoichiometry and structure has emerged recently. Direct evaluation with X-ray methods (XRD, EXAFS, and EDS), as well as indirect evidence such as voltammetry and molecular simulation, suggest that the electroactive NiHCF thin films are quite diverse. The structural analogue of soluble Prussian blue has an ideal Ni:Fe stoichiometery of unity, though typical NiHCF lattices are Ni^{2+}-rich, with a Ni:Fe ratio as large as 1.5. Higher Ni:Fe ratios arise from $Fe(CN)_6^{-3/4}$ lattice vacancies, extra Ni^{2+} occupying interstitial alkali cation sites, or some combination of both.[10−15] In bulk synthesis, processing conditions can be used to tune the stoichiometry and structure of NiHCF powders over the entire range of Ni:Fe stoichiometries,[16] and we have recently shown that bulk powder synthesis methods can be adapted to thin film synthesis.[17] These recent advances in NiHCF thin film processing now make it possible to begin probing the influence of subtle changes in lattice stoichiometry on the resulting intercalation electrochemistry.

* To whom correspondence should be addressed.
† Taiyuan University of Technology.
‡ University of Washington.

(1) de Tacconi, N. R.; Rajeshwar, K.; Lezna, R. O. *Chem. Mater.* **2003**, *15*, 3046−3062.
(2) Bacskai, J.; Martinusz, K.; Czirok, E.; Inzelt, G.; Kulesza, P. J.; Malik, M. A. *J. Electroanal. Chem.* **1995**, *385*, 241−248.
(3) Coon, D. R.; Amos, L. J.; Bocarsly, A. B.; Fitzgerald-Bocarsly, P. A. *Anal. Chem.* **1998**, *70*, 3137−3145.
(4) Rassat, S. D.; Sukamto, J. H.; Orth, R. J.; Lilga, M. A.; Hallen, R. T. *Sep. Purif. Technol.* **1999**, *15*, 207−222.
(5) Lilga, M. A.; Orth, R. J.; Sukamto, J. P. H.; Rassat, S. D.; Genders, J. D.; Gopal, R. *Sep. Purif. Technol.* **2001**, *24*, 451−466.
(6) Jeerage, K. M.; Schwartz, D. T. *Sep. Sci. Technol.* **2000**, *35*, 2375−2392.
(7) Humphrey, B. D.; Sinha, S.; Bocarsley, A. B. *J. Phys. Chem.* **1984**, *88*, 736−743.
(8) Schneemeyer, L. F.; Spengler, S. E.; Murphy, D. W. *Inorg. Chem.* **1985**, *24*, 3044−3046.
(9) Lasky, S. J.; Buttry, D. A. *J. Am. Chem. Soc.* **1988**, *110*, 6258−6260.
(10) Bacskai, J.; Martinusz, K.; Czirok, E.; Inzelt, G.; Kulesza, P. J.; Malik, M. A. *J. Electroanal. Chem.* **1995**, *385*, 241−248.
(11) Kelly, M. T.; Arbuckle-Keil, G. A.; Johnson, L. A.; Su, E. Y.; Amos, L. J.; Chun, J. K. M.; Bocarsly, A. B. *J. Electroanal. Chem.* **2001**, *500* (1−2), 311−321 (Sp. Iss. SI, MAR 16 2001).
(12) Yu, Q.; Steen, W. A.; Jeerage, K. M.; Jiang, S.; Schwartz, D. T. *J. Electrochem. Soc.* **2002**, *149*, E195−E203.
(13) Steen, W. A.; Han, S. W.; Yu, Q. M.; Gordon, R. A.; Cross, J. O.; Steen, E. A.; Seidler, G. T.; Jeerage, K. M.; Schwartz, D. T. *Langmuir* **2002**, *18*, 7714−7721.
(14) Jeerage, K. M.; Steen, W. A.; Schwartz, D. T. *Chem. Mater.* **2002**, *14*, 530−535.
(15) Zamponi, S.; Berrettoni, M.; Kulesza, P. J.; Miecznikowski, K.; Malik, M. A.; Makowski, O.; Marassi, R. *Electrochim. Acta* **2003**, *48*, 4261−4269.
(16) Loos-Neskovic, C.; Fedoroff, M.; Garnier, E. *Talanta* **1989**, *36*, 749−759.
(17) Steen, W. A.; Schwartz, D. T. *Chem. Mater.* **2003**, 15, 2449−2453.

10.1021/cm0515101 CCC: $30.25
Published on Web 10/14/2005

Among the most sensitive electrochemical experiments for detecting differences in NiHCF materials is the reversible intercalation/deintercalation of K^+. When K^+-containing electrolytes are used, two distinct voltammetric peaks often appear; their relative sizes can vary widely depending upon the electrode processing conditions. Recently, the multipeak voltammetry of K^+ intercalation/deintercalation has been tied to NiHCF stoichiometry.[15] Specifically, energy dispersive X-ray spectroscopy (EDS) showed that lower voltage CV peaks occurred in films that were lower in potassium, whereas higher voltage CV peaks occurred in films that were higher in potassium. Electrodes made from bulk powders with approximate stoichiometries $Ni_{1.5}Fe^{III}(CN)_6$ and $KNiFe^{III}(CN)_6$ were used to affirm that the lower voltage CV peak arose from the nonstoichiometric solid whereas the higher voltage peak arose from the nearly perfect 1:1 stoichiometry.

These prior studies explored the electrochemical response at the stoichiometric extremes of Ni:Fe (1:1 and 1.5:1), but not the behavior over the whole range of processable stoichiometries. Here, we seek to take advantage of new NiHCF thin film processing methods that produce a continuum of stoichiometries and use multivariate statistical tools to assess the correlation between stoichiometry and the resulting electrochemical properties. Cyclic voltammetry in K^+-containing electrolytes is used to evaluate the electrochemical character of individual films, and EDS is used to probe the relative amounts of nickel, potassium, and iron in the thin films. Principal component analysis (PCA)[18,19] of combined CV-EDS data shows the direct link between lattice nonstoichiometry and the electrochemical response of NiHCF thin films. Developing analysis tools to understand how material nonstoichiometry affects the electrochemistry of NiHCF is an essential step in the design of more selective, higher performing alkali sensor and separation materials.

Experimental Section

Sample Preparation. Methods for processing bulk and thin film NiHCF with widely varied stoichiometry have been detailed elsewhere.[16,17] A review examining bulk NiHCF synthesis showed that the stoichiometry and structure of the films produced depend profoundly on total concentration of precursor reagents and the order they are mixed.[16] In contrast, a recent study of thin film NiHCF synthesis suggested that precursor composition is more important than mixing order for determining stoichiometry.[17] Nevertheless, we continue to distinguish between mixing diluted Ni^{2+} precursor into more concentrated $Fe(CN)_6^{-3}$ precursor (we call this mixing order Library A) from the mixing of diluted $Fe(CN)_6^{-3}$ precursor into more concentrated Ni^{2+} precursor (we call this Library B); it has never been evaluated whether the (small) mixing-order-induced variations in stoichiometry give rise to appreciable differences in voltammetry. Total precursor concentration is a key variable, so the system has water (solvent) and the two precursor salts as the three main synthesis components. Table 1 lists the 13 different precursor concentrations used. Throughout the text we will denote films grown under specific conditions by the numbered concentration listed in Table 1 and the letter A or B for the mixing order discussed above. As presented in ref 17, the different solution conditions will be presented graphically using a ternary diagram with the concentrated Fe^{III} precursor electrolyte at one apex (40 mM $K_3Fe(CN)_6$), the concentrated Ni^{II} precursor at another apex (40 mM $NiSO_4$ and 0.5 M Na_2SO_4), and the H_2O diluent at the third apex. The different volume fractions of Ni^{II}, Fe^{III}, and H_2O were deposited by pipetting microliter volumes of the components into a 6 mm × 6 mm reagent well created using a PVC tape mask that was adhered to each uniformly roughened (600 grit sandpaper), electrochemically cleaned, platinum. A piece of hydrophobic PVC film was placed over each substrate to spread the mixture solution uniformly across the reagent well. The samples were left in a room temperature, water-saturated chamber for several hours while the NiHCF film nucleated and grew on the roughened electrode. After NiHCF film growth, the PVC film was removed and another identical deposition was performed. Three rounds of deposition were performed for each substrate to ensure adequate film thickness for good signal-to-noise with EDS.

Table 1. Thirteen Different Nickel Hexacyanoferrate Thin Film Growth Solution Compositions Were Used, though the Reagent Mixing Order Was Varied[a]

	$NiSO_4$, Na_2SO_4 (mM)	$K_3Fe(CN)_6$ (mM)
1	4, 50	8
2	8, 100	4
3	12, 150	12
4	4, 50	24
5	12, 150	16
6	16, 200	12
7	24, 300	4
8	8, 100	28
9	28, 350	8
10	4, 50	36
11	16, 200	24
12	24, 300	16
13	36, 450	4

[a] For mixing order A, the tabulated solution compositions were made by diluting concentrated nickel precursor (40 mM aqueous $NiSO_4$, 0.5 M Na_2SO_4) with varied amounts of water, followed by addition of concentrated iron precursor (40 mM $K_3Fe(CN)_6$). Mixing order B added water diluent into the concentrated iron precursor first and then added concentrated nickel precursor to achieve the final concentration.

Electrochemistry. All electrochemical experiments were performed using a PAR 273A Potentiostat controlled by custom LabVIEW software. Working electrodes were prepared as described above. A platinum wire was used as the counter electrode and all reported potentials are referenced to a saturated calomel electrode (SCE).

After film growth, each sample was cycled 15 times in 1 M KNO_3 solution from 200 to 800 mV at 25 mV/s. Preconditioning assured that films were fully intercalated with K^+ and subsequent CVs were stable (metal hexacyanoferrates sometimes undergo structural transformations upon initial potential cycling, requiring a few cycles to achieve stable response[1]). Each sample was then rinsed with distilled H_2O and cycled 15 more times in fresh 1 M KNO_3 electrolyte; the final CV was used as the characteristic CV for each electrode. After preconditioning, samples were placed in their oxidized state by holding the potential at 800 mV vs SCE for 15 min, then emersed from solution while under potential control, quickly rinsed, and dried in air.

Energy Dispersive X-ray Spectroscopy (EDS). Oxidized films were analyzed using EDS. A scanning electron microscope (JEOL JSM-5200) operated at an accelerating voltage of 15 keV was used to acquire EDS spectra of the sample. Spectral background was subtracted using a locally weighted least-squares regression technique, and the peaks were fit to a Gaussian function. All reported spectra were normalized using Fe, the species responsible for

(18) Wold, S.; Esbensen, K.; Geladi, P. *Chemometr. Intell. Lab. Syst.* **1987**, *2*, 37−52.
(19) Steen, W. A.; Jeerage, K. M.; Schwartz, D. T. *Appl. Spectrosc.* **2002**, *56*, 1021−1029.

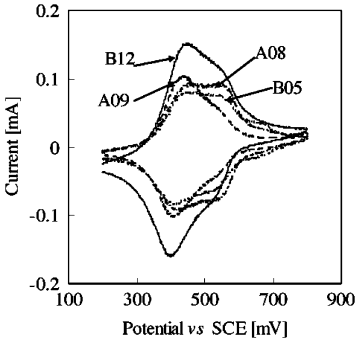

Figure 1. Cyclic voltammograms for four different electrodes processed under the synthesis conditions A08, A09, B05, and B12 (see Table 1). The final preconditioning CV is shown.

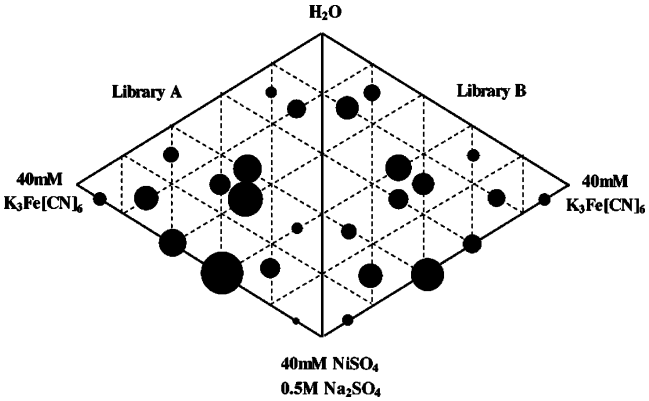

Figure 2. Charge densities for each sample are plotted on a ternary diagram that shows the volume fraction of each component in the synthesis solution (final compositions are presented in Table 1). Two different reagent mixing orders, Libraries A (left) and B (right), are plotted side by side (see text). The diameter of each black dot is proportional to the film charge density.

electroactivity, as an internal standard. The EDS detector allowed us to analyze Ni, Fe, and K, but not light elements C and N. All films had strong Pt substrate signal, but we have excluded that part of the energy spectrum; strong substrate signal indicates thin-film EDS analysis assumptions should be valid here.

Results

Electrochemistry and EDS. Figure 1 is a plot of the final cyclic voltammogram (CV) from the preconditioning step for four different electrodes. Positive currents correspond to the oxidation of NiHCF with K^+ deintercalation from the matrix and negative currents denote reduction with K^+ intercalation. Figure 1 shows that the different film preparation procedures for each electrode sample leads to quite different reversible charge densities and CV shapes; the two distinct CV peaks discussed in the Introduction are clearly seen, with the peaks separated by roughly 100 mV. The different processing conditions for each electrode also leads to different charge densities (found by integrating the final preconditioning voltammogram). Processing condition A12 creates films with the largest charge density (q_{A12}), so it is used to normalize all the other conditions to get the relative charge density, $x_i = q_i/q_{A12}$ for each sample *i*. Figure 2 shows values of x_i, with larger circles corresponding to greater charge densities. The ternary diagrams for the two libraries are plotted edge-to-edge to better show symmetry in the synthesis conditions; one sees that the high-capacity samples in Library A also tend to be high in B. Samples in the middle

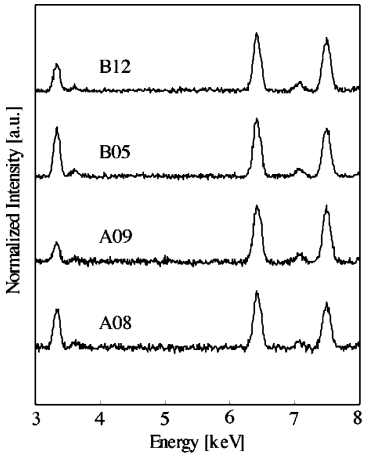

Figure 3. Fe-normalized EDS spectra for the same NiHCF samples shown in Figure 1.

of the diagram generally have higher capacity, whereas thin films from Fe^{III}-rich or Ni^{II}-rich growth conditions are usually low. Variations in charge density can arise from differences in film thickness, differences in material stoichiometry, or more likely, a combination of stoichiometric and thickness variations.

Energy-dispersive X-ray (EDS) analysis is a straightforward way to get at the relative stoichiometries of different films. Figure 3 shows the oxidized-state EDS spectra for the same electroactive NiHCF samples shown in Figure 1. The main Kα X-ray emission peaks are at 3.3 keV for intercalated K ions, 6.4 keV for Fe, and 7.5 keV for Ni (small Kβ peaks are also seen at 3.6 and 7.1 keV for K and Fe, respectively). Each spectrum in Figure 3 is normalized to give identical integrated Fe Kα peak intensities. Because the incident electrons easily penetrate the entire NiHCF film (as evidenced by large substrate signal at energies not shown), we can use a straightforward thin film analysis where (to leading order) the elemental composition is proportional to the signal intensity (see details in refs 6 and 14). In the thin film limit, normalizing with the Fe EDS intensity is identical to normalizing the electrochemical response with the films charge density since all irons in a fresh film are redox active.[19] Thus, relative stoichiometries can still be determined, but the influence of film thickness is removed.

A common defect structure in NiHCF involves lattice vacancies on the octahedrally coordinated $Fe(CN)_6^{-3/4}$ sites; we denote the number of these vacancies per unit cell *n*. Nonstoichiometric films can also result from interstitial Ni^{2+} located in the alkali cation sites; we denote the number of these interstitials *m* per unit cell. When these are the only defects, the unit cell stoichiometry for a fully oxidized film is

$$K^{I}_{4-3n-2m}Ni^{II}_{4+m}[Fe^{III}(CN)_6]_{(4-n)} \quad (1)$$

The charge neutrality constraint $3n + 2m \leq 4$ sets a bound on the maximum lattice nonstoichiometry (i.e., Ni:Fe of 1.5:1), assuming only cations and water intercalate into the structure. In the thin film EDS limit used here, the K:Fe intensity ratio is $I_K/I_{Fe} = K_1*(4 - 3n - 2m)/(4 - n)$ and the Ni:Fe ratio is $I_{Ni}/I_{Fe} = K_2*(4 + m)/(4 - n)$, where K_1 and K_2 are proportionality constants that take into account the

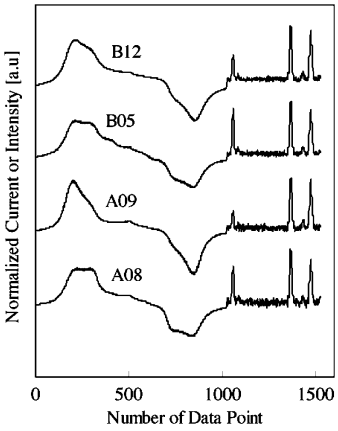

Figure 4. Four composite CV-EDS data vectors for the NiHCF thin films shown in Figure 1 and Figure 3. A total of 59 such data vectors were used for PCA.

X-ray emission physics for each material as well as instrumental factors. Eleven samples in Library A had adequate EDS signal-to-noise, but only 10 samples in Library B. The ratios of I_K/I_{Fe} in the EDS spectra for the 21 samples range from close to 0 (A7) to greater than 1 (A11, A4, B10). These EDS results indicate substantial variation in the parameters *n* and *m* given in eq 1; they also show that the small area array-based synthesis methods used in ref 17 readily scale to larger area electrodes.

It is important to note that eq 1 implies that two NiHCF films can have identical stoichiometry but very different structures. Hence, prior work showing modest effects of precursor mixing order on the stoichiometry of thin film NiHCF[17] does not ensure that the resulting films had the same structure nor did these prior results evaluate the electrochemical response among nominally identical stoichiometries.

Principal Component Analysis (PCA). To correlate the stoichiometry and the electrochemical behavior of NiHCF thin films prepared under different experimental conditions, electrochemical and EDS data are analyzed simultaneously using principal component analysis (PCA). A set of composite data vectors were created by combining the current density data from cyclic voltammograms (e.g., Figure 1) with the oxidized-state EDS spectra (e.g., Figure 3) for each electrode. Four composite data vectors are shown in Figure 4, built from the data presented in Figures 1 and 3. A total of 59 composite CV-EDS data vectors were made. Qualitatively, the four composite CV-EDS curves shown in Figure 4 appear to link the size of the K EDS peak in oxidized NiHCF with the CV shape; more K is present when the ratio of high voltage-to-low voltage CV peak is larger. A linear fit of K EDS peak height vs CV peak ratio for the full 59 CV-EDS data vectors confirms the qualitative trend seen in Figure 4, but this univariate fit only captures 14% of the variance in the EDS data, ultimately making the relationship between CV shape and K EDS data ambiguous. Multivariate analysis like PCA provides greater robustness and lower sensitivity to outliers, clarifying any statistically significant correlation among variables.

Before analyzing the data with PCA, it is important to elaborate on some of the details associated with the construction and normalization of the composite CV-EDS data. Electrochemical response is a spatially averaged property from an entire electrode, whereas EDS spectra are local. To accommodate this difference, EDS spectra were acquired at several locations on each electrode, providing a total of 59 spectra from 21 different electrodes. A composite data vector was made from each spectrum using the CV from that electrode. Data normalization is needed to ensure that the CV and EDS data of each composite vector received approximately equal weighting. Several normalization schemes were evaluated in preliminary studies, with the following procedure providing the most uniform weighting of variables:

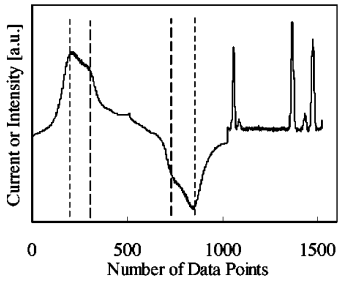

Figure 5. Mean CV-EDS data vector for all 59 data files. Vertical dashed lines denote the regions where the low-voltage (short dash) and high-voltage (long dash) CV peaks appear.

1. Normalize all EDS spectra so their integrated Fe intensity was unity.

2. Normalize all cyclic voltammograms so their integrated current in the positive half of the voltammogram was ten.

3. Append each normalized EDS spectrum to the normalized CV data for that particular electrode.

4. The data were mean-centered. Mean centering involves subtraction of the mean data vector from the 59 individual CV-EDS data vectors. Figure 5 shows the mean CV-EDS vector.

This normalization procedure ensured that the magnitudes of important EDS and CV variables were comparable; the units on a variable (counts or current) do not matter in PCA, just magnitudes. The difference in integration factors for the Fe EDS signal (unity) and the voltammogram (ten) ensured that the Fe EDS peak and CV peaks were comparable in magnitude and, thus, comparably weighted, in each data vector. The specific multiplier (ten) recognizes that the average CV peak width is approximately 10-fold broader than the Fe EDS peak width in each data vector. With fixing of the proportion of Fe EDS signal and CV integrated peak area in each sample, gross film thickness effects are also removed since the Fe EDS signal and the film redox activity are both linearly proportional to the amount of Fe in the film.

PCA was performed on the matrix of 59 mean-centered CV-EDS vectors in order to segregate the data along the dimensions of greatest variance, i.e., the eigenvectors of the data matrix (called the Loadings), and to determine the magnitude of each eigenvector (called the Scores)[18,19] We used the PLS Toolbox (Eigenvector Inc.), a chemometrics analysis package for Matlab, to perform the computations. Figure 6 shows the first two principal component (PC) Loadings vectors and variance percentage captured by each principal component (PC). About 50% of all the variance in the data is captured by the first principal component. An

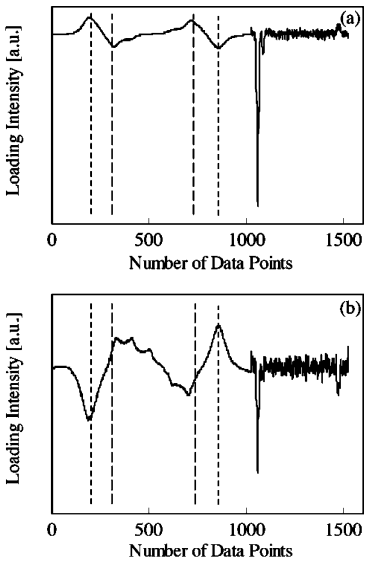

Figure 6. Principal component loadings vectors for (a) PC1 and (b) PC2. Vertical dashed lines denote the regions where the low-voltage (short dash) and high-voltage (long dash) CV peaks appear.

additional 22% of the variance is captured by PC2. All other PCs are small and mostly capture noise.

Interpretation of the loading vectors is aided by the dashed lines in the mean data vector (Figure 5) and in the PC1 loading vector (Figure 6a). The short-dashed lines in Figure 5 are the locations in the data set where the low-voltage CV redox peaks occur (oxidation peaks are positive and reduction peaks negative). The long-dashed lines correspond to the location where the higher voltage redox peaks occur; these locations are also marked in the PC1 and PC2 Loading vectors (Figure 6). One observes features in the PC1 Loading vector at the same locations where the high- and low-voltage peaks occur in the mean vector. The low-voltage features in Figure 6a (short dash) always deviate in the opposite direction from the high-voltage features (long dash), meaning the two peaks are negatively correlated. At the same time, the EDS portion of the PC1 Loading shows a large negative peak at the location corresponding to the K EDS signal and a small positive peak at the location for the Ni signal. The fact that the K and Ni portion of the EDS spectrum are negatively correlated with one another is consistent with the stoichiometric relationship presented in eq 1; an increase in the Ni:Fe ratio will be accompanied by a decrease in K. Taken together, the Loading for PC1 shows that when the CV has a large low-voltage intercalation peak, it will have a small high-voltage peak, less intercalated K, and a larger than average Ni:Fe ratio in the NiHCF film (i.e., greater nonstoichiometry). Of course, the opposite is also true: A smaller than average lower voltage CV peak is correlated with a larger high-voltage peak and less nonstoichiometry (a lower Ni:Fe ratio). This matches what we observed qualitatively in Figure 4.

The Loading for PC2 (Figure 6b) represents a significantly more complex interaction between stoichiometry and voltammetry. Prominent features in the voltammetry region of PC2 are seen to align very well with the low-voltage peak (short-dashed lines), but not as well with the high-voltage peak (long-dashed lines). Moreover, the K and Ni portion of the EDS signal move in tandem, unlike the features observed in PC1. The tandem motion of K and Ni EDS signals is somewhat surprising given that the stoichiometry of eq 1 indicates these should always be negatively correlated to maintain charge neutrality (as we see in PC1). In short, even though PC2 captures significantly less variance in the data, it perhaps provides a glimpse into a more subtle set of interactions.

Discussion

PC1, which describes more than 50% of all the variance in the data set, shows that the lower voltage reversible CV peaks correlate to K^+ intercalation into more nonstoichiometric lattices, whereas the higher voltage peak is from intercalation into a low defect lattice. Based on the difference in potential between the peaks, the two types of intercalation sites (those associated with nonstoichiometric defects and those associated with a more stoichiometric lattice) have a Gibb's energy difference of $\Delta G \approx 10$ kJ/mol. Most significantly, the Loading for PC1 (Figure 6a) shows that the location (energy) of the low- and high-voltage intercalation peaks do not shift (to first approximation) as the level of nonstoichiometry is widely varied among the samples. The fact that the relative proportion of the two intercalation peaks changes, but not their locations, implies that the different intercalation sites are largely noninteracting. Molecular dynamics (MD) simulations performed previously (for Cs^+, Na^+, and water intercalation) showed that the energetics of the intercalated solid (and, hence, the voltammetry) is strongly dependent on nonstoichiometry from $Fe(CN)_6^{-3/4}$ lattice vacancies (conditions $n = 0$, $n = 1$, and $n = {}^4/_3$ were studied with $m = 0$).[12] However, these simulations showed that the lattice is quite effective at screening steric and Coulombic interactions between neighboring intercalation sites. Thus, it is perhaps not surprising that, to a first approximation, intercalation sites in NiHCF do not interact strongly.

The fact that the Loading for PC2 (Figure 6b) shows the higher voltage peak shifted from the mean centered data (Figure 5) and PC1 (Figure 6a), as well as a positive correlation between the K and Ni EDS peaks, may suggest that there are subtle secondary interactions among the intercalation sites that lead to modulation of the higher voltage intercalation peak. However, for the small data set (59 CV-EDS vectors) analyzed here, we hesitate to overanalyze low-variance PCs since they are prone to display features that arise from a small number of anomalous data sets.

Conclusions and Implications

We have used cyclic voltammetry and energy dispersive X-ray spectroscopy to show that variations in NiHCF thin film stoichiometry can be used to change the relative proportion of a lower energy and a higher energy K^+ intercalation site. The energetics of these two intercalation sites are largely independent of the concentration of the two sites, implying the NiHCF lattice screens Coulombic and steric interactions between the sites.

This work has important implications for the engineering of more sensitive alkali cation sensors and electrochemically

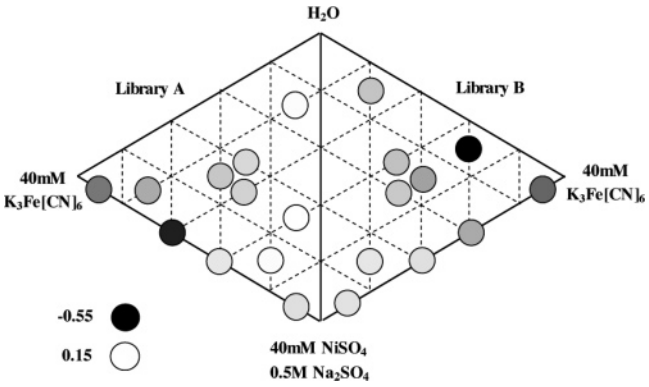

Figure 7. Score values for PC1 are placed on the ternary processing diagrams for mixing Libraries A and B to show the relationship between processing and NiHCF stoichiometry (the more negative the Score, the fewer the defects, and vice versa).

switched ion exchange schemes. For an ideal sensor or separation matrix, one would seek thin film processing conditions that produce a film with predominantly one type of intercalation site or the other, rather than a mixture of both. To begin understanding optimal conditions for this synthesis, Figure 7 presents the PC1 Score values for all 59 data sets evaluated in this study. Each of the CV-EDS data vectors has a PC1 Score value that multiplies the PC1 Loading vector (Figure 6a) to indicate how a specific data vector deviates from the mean CV-EDS data vector (Figure 5). The more positive a PC1 Score value, the more that sample has the characteristics of nonstoichiometric (high Ni:Fe) NiHCF; the more negative the PC1 Score, the more closely the film approaches the perfect 1:1 Ni:Fe stoichiometry. In Figure 7, the most positive Score is pure white and the most negative Score is black. The Score plot shows that the most stoichiometric solids are from high iron synthesis whereas low iron growth conditions lead to greater nonstoichiometry (higher Ni:Fe ratios in the films). The two mixing libraries display reasonably good symmetry, indicating that mixing order has a secondary effect on the electrochemistry of the resulting films.

One cannot say, a priori, whether a low- or high-defect lattice will be best for a particular mixture of alkali cations to be detected or separated; that determination will require individual testing. Nonetheless, this work clearly shows that one need only screen the most and least stoichiometric materials to make that evaluation because all intervening defect concentrations are to first approximation a linear (largely noninteracting) combination of the two lattice compositions. In short, these results should help accelerate the development of more optimized materials.

Acknowledgment. Professor Xiaogang Hao gratefully acknowledges support provided by the Chinese Scholarship Council to spend a year at the University of Washington. This research was supported in part by National Science Foundation Grant CTS-0236608.

CM0515101